Left Ventricle Volume Measuring Using Echocardiography Sequences

Yi Guo, Simon Green, Laurence Park and Lauren Rispen
Western Sydney University
Penrith, NSW 2750, Australia
y.guo, s.green, l.park,l.rispen@westernsydney.edu.au

***Abstract*—Measuring left ventricle (LV) volume is a challenging problem in physiological study. One of the non-intrusive methods that is possible for this task is echocardiography. By extracting left ventricle area from ultrasound images, the volume can be approximated by the size of the left ventricle area. The core of the problem becomes the identification of the left ventricle in noisy images considering spatial temporal information. We propose adaptive sparse smoothing for left ventricle segmentation for each frame in echocardiography video for the benefit of robustness against strong speckle noise in ultrasound imagery. Then we adjust the identified left ventricle areas (as curves in polar coordinate system) further by a fixed rank principal component analysis as post processing. This method is tested on two data sets with labelled left ventricle areas for some frames by expert physiologist and compared against active contour based method. The experimental results show clearly that the proposed method has better accuracy than that of the competitor.**

***Index Terms*—Echocardiography, image segmentation, function smoothing**

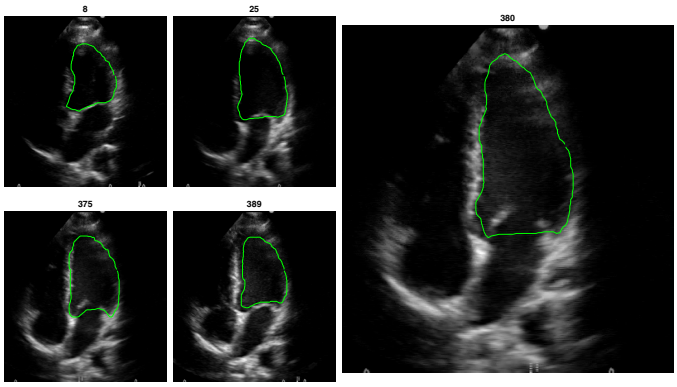

Fig. 1: Sample frames from one ultrasound video sequence with frame number on top.

1. Introduction

Measuring the volume of left ventricle (LV) from echocardiography video sequences has many applications in physiological research. For example, the subject is tested under different breathing conditions and ultrasound images are consistently sampled in situ to monitor the stroke volume. The data is the video sequences of the heart and our focus is the volume of the left ventricle in each image. Since the imaging is done in 2D, we use the area of the left ventricle as a surrogate for volume. Although this is only an approximation, in most circumstances, this approximate will be good enough for example when the change of heart volume under different conditions is of interest.

Some sample frames are shown in Fig. 1, which shows ultrasound images of the four chambers of the heart in the so-called apical four-chamber (A4C) view. These images are original ultrasound images without any processing. Note that the conventional display in echocardiography is upside down and with the left and right switched. So LV is on the right side, labelled by green curve in the figure. These images typify common problems with echocardiography that present challenges with image analysis, such as 1) variable clarity of the image, most places blurry, 2) loss of visibility of some tissues such as some fraction of an external ventricular wall, and 3) speckling every where especially in the LV chamber.

If we focus only on LV area, it is not quite clear where the true LV internal wall should be even for humans. The delineated LV boundaries, green curves in Fig. 1, was generated manually by expert physiologist. The target is to design an automated system to extract LV area, i.e. delineating the internal wall of LV and calculating its area, which could hopefully agree with what experts will obtain.

Apparently this can be treated as an object identification and tracking problem in computer vision. Indeed, there are many papers about left ventricle tracking for different data modalities using various methods, such as magnetic resonance imaging (MR) sequences [14, 1, 2], computerised tomography (3D ultrasound) [18], and 2D echocardiography [13, 15, 14]. Most of them are dealing with the images in the original image domain. The usual workflow is image enhancement such as despeckling [17] and noise reduction [19], then segmentation [8] and then temporal correlation [6, 3].

Nonetheless, we treat it as an image-based object identification problem instead of a tracking problem. There are many shape-based methods such as active contour and snake [7]. They are working on original image and searching for image statistics such that the region of interest (ROI), i.e. the entire LV, has distinct features from other areas. In this paper we describe a novel method which uses polar coordinates instead where the segmentation problem is converted into a function smoothing problem so that a specific smoothing scheme can be designed to tackle problems that may arise. The advantage of this conversion is that it does denoising and segmentation at once and thus reducing the pressure from image preprocessing.

978-1-5386-6602-9/18/$31.00 ©2018 IEEE

Moreover, based on the knowledge of the cardiac cycle, we propose fixed rank principal component analysis (PCA) to further smooth the identified LV areas so that these areas are similar to each other and their corresponding curves occu three subspaces each of which is a phase in a cardiac cycl

The following sections will explain the method in m detail, followed by some experiments to show its effectiven

2. Polar coordinates

Write I as a given image, p the pixel values. Before conversion, an image of an echocardiography sequence has to pass a simple image enhancement. We use adaptive histogram equalisation [11] with 1024 bins and 8×8 tiles. Then the image is binarised by thresholding at $\bar{p} + 2\sqrt{Var(p)}$, where $\bar{p}$ and and $Var(p)$ are the mean and variance of all pixels. Then we apply "close" and "clean" morphological operations to remove isolated pixels. Fig. 2 shows the processed image at each step.

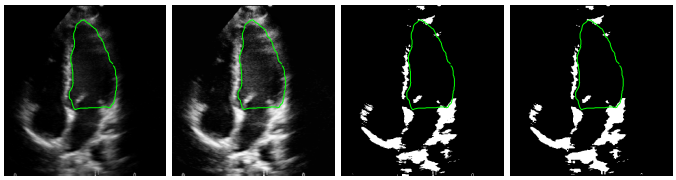

Fig. 2: One image (frame 380 shown in Fig. 1) from the sequence. From left to right, the image passes through three simple steps for image preprocessing.

It is clear that some fraction of the left ventricle is missing while most of it is preserved. The chamber of the left ventricle is the dark area in the middle. If one locates the origin of polar coordinate system inside the left ventricle chamber, and convert the usual Cartesian coordinates of remaining pixels (see the fourth plot in Fig. 2) to polar coordinate system, then the pixels in the new coordinate system will lie above a base line, which is the boundary of the left ventricle. In echocardiography, it is usually straightforward to find a point inside the chamber. It can be estimated or set manually so that despite lateral movement of the heart, it will remain within the LV chamber. It matters little where the origin of polar coordinate system because it changes only the shape of the boundary but not the relative locations of the pixels. We write $l(\theta)$ for a pixel in polar coordinates, emphasising the value of l, the distance, as a function of the angle θ and $\theta \in [0, 360^o]$. Fig. 3 shows a binarised frame and two sets of polar coordinates at different origins (as blue and green crosses). The two sets are very similar and therefore it is not critical in regards to where the origin is as long as it is inside LV chamber. Interestingly the inner wall of the LV chamber now becomes the lower boundary of all pixels in polar coordinate system. Finding this lower boundary is a much easier problem than delineating the inner wall of LV in image. Although there are many LV inner wall pixels missing, it would be easier in this domain to "patch up" by simple interpolation. In following discussion, we assume all operations are in polar coordinate system and clarify it otherwise.

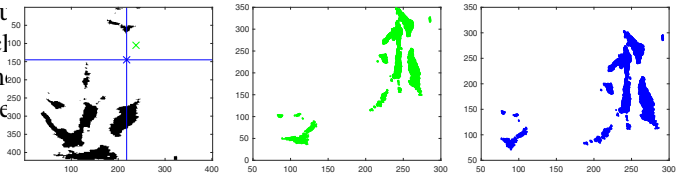

Fig. 3: The binary image of frame 380 shown in Fig. 1 with bins (blue lines). Left: the binary image with two origins (blue and green crosses); middle and right: the polar coordinates of remaining pixels centred at blue and green crosses respectively; horizontal axis is angle from 0 to 360 degrees and and vertical is distance from the origin.

3. Adaptive Sparse Smoothing

Due to the nature of raster scan in image, the pixels in polar coordinates are also in discrete "grid" as shown in the right panel in Fig. 4, which is a detailed plot of a section at angles between 233-243 degrees. As the inner wall of LV is connected elastic muscular tissue, it should be smooth without sharp turns and in general no drastic changes so that the boundary pixels in image in polar coordinates should be smooth as well. The green dotted line in Fig. 4 shows an estimation of the LV wall delineated manually by human expert, which is regarded as ground truth. We start with rough estimation of LV wall as

$$y_b(\theta_b) = \min\{l(\theta),\ \forall\theta \in [\theta_b, \theta_{b+1})\}, \tag{3.1}$$

where $b = 1, \ldots, B$ is the index of total B equal width angles bins, and θ_b and θ_{b+1} are both sides of the bth bin. Note that y_b's have values only on θ_b's. This amounts to down sampling on the image to reduce dimensionality. However, it is straightforward to extend to all pixels by setting $y(\theta) = y_b(\theta_b)$ when $\theta \in [\theta_b, \theta_{b+1})$. We set $B = 200$ throughout the paper although this number can be optimised. As B increases, y becomes less smooth.

The red dotted line in Fig. 4 shows the estimated lower boundary y, or in other words, a rough estimate of the LV wall. The departure of this estimate from the true one is quite clear, with large changes at various places, e.g. the most noticeable at 237 degrees, non-smoothness and missing values. Nevertheless, the section around 160∼210 degrees is good and the section 130∼160 degrees appears noisy.

There are several observations from this simple estimation. A. if one could filter out the large changes, the fit (to the true LV wall) would be reasonable. B. some sections can be fixed by smoothing such as 130∼160 degrees section. C. the missing part can be filled by interpolation, even as simple as linear interpolation if both ends of the missing section can be well fitted. D. the pixels above the boundary have little influence to the determination of the boundary.

Considering the requirement of filtering large changes, we introduce sparsity in the smoothing model. Write $\mathbf{y}$ as the vector form of the rough estimate of LV wall with missing

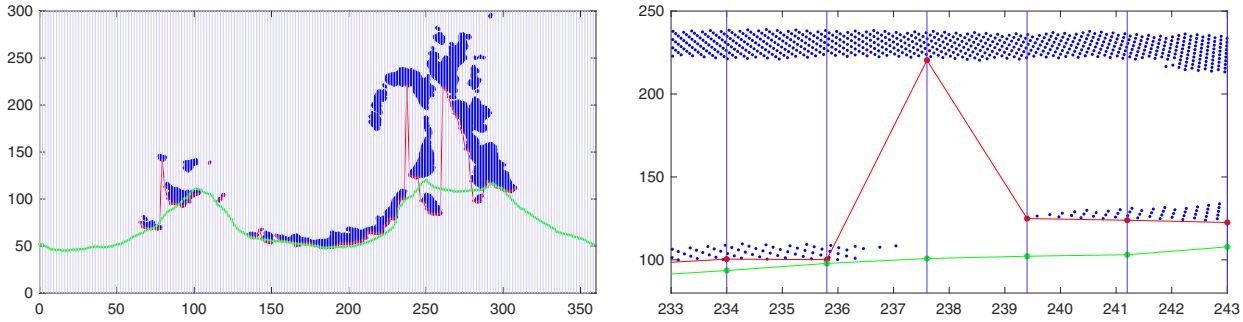

Fig. 4: The image (frame 380 in Fig. 1) from the sequence. The red dotted line is the estimated lower boundary and green one is the ground truth. Left: the image in polar coordinates with bins (light blue bars); right: the section of left plot at angles between 233-243 degrees.

values removed, and $\mathbf{f}$ the smoothed version. We have the following model

$$\mathbf{y} = \mathbf{f} + \boldsymbol{\epsilon}, \quad \boldsymbol{\epsilon} \sim \mathcal{L}(\boldsymbol{\theta}) \tag{3.2}$$

where $\boldsymbol{\epsilon}$ is the noise, $\mathcal{L}(\boldsymbol{\theta})$ is Laplacian distribution with parameters $\boldsymbol{\theta}$, and $\mathbf{f} \in \mathcal{C}^1$ a family of smooth functions with continuous derivative of at least order 1, for example splines. The purpose of modelling noise with Laplacian distribution is to increase the probability of large changes so that the model will not move too much to deal with them. The next is to write a maximum likelihood (ML) function for parameters estimation and then maximum a posterior to obtain $\hat{\mathbf{f}}$. However, we take another route to achieve the same thing as the following

$$\min_{\mathbf{f}} \|\mathbf{y} - \mathbf{f}\|_1 + \lambda S(\mathbf{f}), \tag{3.3}$$

where $\|\cdot\|_1$ is the ℓ_1 norm of a vector, $S(\cdot)$ is the smoothness evaluation function, and $\lambda \geq 0$ is a regularisation parameter. We choose $S(f) = \|\mathcal{D}(f)\|_2^2$ where $\mathcal{D}$ is the differentiation operator and $\|\cdot\|_2$ is the ℓ_2 norm. It is well known that (3.3) is equivalent to the probabilistic scheme through ML [9] while it has more direct interpretation in that the ℓ_1 norm for the noise has some tolerance for large values, and the second term is the trade-off between fit and smoothness. We call it sparse smoothing or SPAS for short.

We introduce $\mathbf{x} = \mathbf{y} - \mathbf{f}$ and (3.3) becomes

$$\min_{\mathbf{x}} \|\mathbf{x}\|_1 + \lambda \|\mathcal{D}(\mathbf{x} - \mathbf{y})\|_2^2, \tag{3.4}$$

which is readily solved by many optimisation schemes. We use gradient projection [12] for it. The above problem is convex. Therefore a unique solution exists and the initialisation is not critical.

Fig. 5 shows the results of SPAS with various values of λ. SPAS successfully screens large sudden changes such as large spikes thanks to its robustness brought by the sparse component. Apparently, the larger the value of λ, the smoother the estimated curve. Although smoother is not necessarily better as the SPAS with $\lambda = 5$ has significant departure from truth at many places such as around 100 degrees, it is

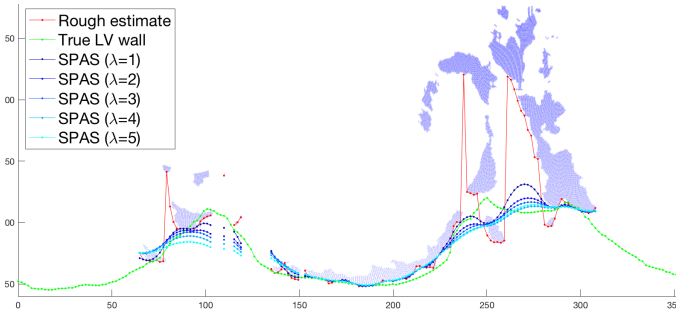

Fig. 5: The image (frame 380 in Fig. 1) from the sequence. The red dotted line is the estimated lower boundary and green one is the ground truth.

preferable to have stronger smoothing effect at some places such as at 259 degree where the largest jump happens caused by missing pixels so that the left atrium's inner pixels are mistakenly picked up as LV wall. This clearly requires an adaptive scheme of smoothing.

We introduce adaptive smoothing for the both terms in Eq. (3.3) as

$$\min_{\mathbf{f}} \|\mathbf{W}_f(\mathbf{y} - \mathbf{f})\|_1 + \beta \|\mathbf{W}_s \mathcal{D}(\mathbf{f})\|_2^2, \tag{3.5}$$

where $\mathbf{W}_f$ and $\mathbf{W}_s$ are diagonal matrices with compatible sizes containing penalty weights for noise and smoothness. Write $\mathbf{w}_f$ and $\mathbf{w}_s$ the vectors consisting of diagonal elements of $\mathbf{W}_f$ and $\mathbf{W}_s$ respectively, $\hat{\mathbf{f}}_1(\lambda)$ the solution of (3.3) at λ and $\hat{\mathbf{n}}_1 = \mathbf{y} - \hat{\mathbf{f}}_1(\lambda)$. Then we set

$$\mathbf{w}_f = \frac{Mean(|\hat{\mathbf{n}}_1|)}{|\hat{\mathbf{n}}_1|} \tag{3.6}$$

and

$$\mathbf{w}_s = \max\{1, \frac{|\hat{\mathbf{n}}_1|}{Mean(\hat{\mathbf{n}}_1)} - 1\} \tag{3.7}$$

where $Mean(\mathbf{x})$ is the mean of $\mathbf{x}$. Eq. (3.6) is similar to the weights in a single iteration of re-weighted ℓ_1 minimisation [5]. However we use Eq. (3.6) as the weights in lieu of $\frac{1}{|\hat{\mathbf{n}}_1| + \epsilon}$ in [5]. Apparently Eq. (3.6) is more conservative in terms

of sparsity encouraging ability as the smaller ones are not so heavily penalised. Note that if we assume the noise from Laplacian distribution with zero mean, $Mean(|\hat{\mathbf{n}}_1|)$ is the mean absolute deviation, i.e. the bandwidth of the distribution. Then Eq. (3.6) is a standardisation of the noise to have unit bandwidth. From this point of view, the function of Eq. (3.7) is then quite clear. A "normal" amount of smoothing applies to places where the noise (after standardisation) is within one unit, otherwise the smoothing effect increase proportionally with the deviation from unit length. The purpose of these two sets of weights together is to smooth across large gaps such as the one at 260∼280 degrees shown in Fig. 5. The gap is caused by the mitral valve flipping up to fill LV. Part of it is missing during binarisation (see the little "island" at around 250 degrees in Fig. 5). The lower boundary finding, i.e. (3.1), then "sees" through to left atrium (LA) wall and causes th big jump. Then later boundary section (after 250 degrees) i actually LA wall pixels until LV wall back in sight at 29(degrees. The weights in (3.6) and (3.7) work together so tha the large jump can be ignored and strong smoothing effect after the big jump ensures that the final curve can get across the gap without mounting back the erroneous pixels. We call (3.5) adaptive sparse smoothing (ADASPAS).

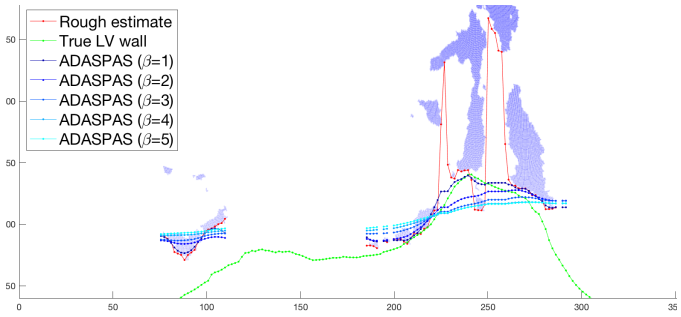

Fig. 6: The image (frame 380 in Fig. 1) from the sequence. The red dotted line is the estimated lower boundary and green one is the ground truth.

Fig. 6 shows the results of ADASPAS with various values of β with $\lambda = 5$ in the first pass to obtain $\mathbf{W}_f$ and $\mathbf{W}_s$. The fit is much better at the big gap while almost the same as SPAS at other places. Similar to λ in SPAS, β in ADASPAS is controlling the trade-off between noise reduction and smoothness. As we can see from Fig. 6, too strong smoothing is not desirable as the outcome lacks the ability to trace the LV wall pixels. The choice of λ and β has to be carried out carefully to ensure good result. We fix $\beta = 1$ and $\lambda = 5$ in our experiments as this set seems to work reasonably well. The optimal value of λ and β is a topic of our future research.

After ADASPAS, we obtain an estimation of LV wall in polar coordinates, where there is still a missing value issue. It can be done in either polar coordinate system or in Cartesian coordinate system. We choose the latter as line segment in polar coordinates is section of parabola in Cartesian coordinates, which tends to overestimate the LV area. Therefore, we convert from polar coordinates to Cartesian resulting segments of estimated LV walls on the original image. The missing pieces are filled then by connecting both ends.

Fig. 7 shows the final segmentation of LV on frame 380. It is very challenging as a large portion of the LV wall is missing and the mitral valve pixels have to be removed ideally. The rough estimation, shown in the 2nd from left in Fig. 7, stretched outside of LV and into the left atrium due to the missing pixels after binarisation. ADASPAS smoothes out those large spikes and gets through the gap where the mitral valve should be, i.e. the bottom of LV. The estimated area is similar to the expert's estimate.

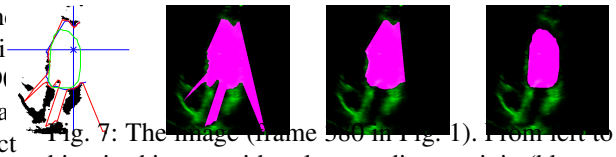

Fig. 7: The image (frame 380 in Fig. 1). From left to right: the binarised image with polar coordinate origin (blue cross) along with roughly estimated (red curve), ADASPAS refined LV boundaries (blue) and ground truth contour (green); roughly estimated LV area rendered in image (pink area); ADASPAS estimated LV area; ground truth LV area.

4. Fixed Rank PCA

It is known that the cardiac cycle has four stages in terms of blood flow, i.e. isovolumic relaxation, inflow, isovolumic contraction and ejection [10]. Therefore in each stage, the left ventricle can be regarded as contracting or expanding concentrically which will be reflected as vertical shift if we assume the centre does not move. Let $\mathbf{f}_i$ be the estimated LV wall curve for the ith frame in the video after missing values filled, $\mathbf{F} = [\mathbf{f}_1, \ldots, \mathbf{f}_N]$ the matrix of all LV. Based on the stages in cardiac cycle, each stage could be a subspace where the LV wall looks very similar except vertical shift, and therefore a rank 1 subspace. Given 4 stages, we conjure that the underlying subspace is actually of rank 4, so we have the following model

$$\mathbf{F} = \mathbf{C} + \mathbf{E}, \quad Rank(\mathbf{C}) = 4 \tag{4.1}$$

where $\mathbf{C}$ is the matrix of true LV wall curves and $\mathbf{E}$ is the error matrix and both are of compatible size to $\mathbf{F}$. For robustness consideration, we again apply sparse encouraging norm to $\mathbf{E}$ to quantify the error, which leads to the following problem

$$\begin{aligned} &\min_{\mathbf{E},\mathbf{C}} \|\mathbf{E}\|_1 \\ &s.t.\ Rank(\mathbf{C}) = 4 \\ &\mathbf{F} = \mathbf{C} + \mathbf{E} \end{aligned} \tag{4.2}$$

which is called fixed rank PCA. The rank constraint causes the objective in (4.3) NP-hard and therefore we have to seek approximation. A feasible approximation is replacing rank by

nuclear norm resulting in robust PCA (RPCA) [4]. Then the objective in (4.3) becomes

$$\min_{\mathbf{E},\mathbf{C}} \|\mathbf{E}\|_1 + \lambda\|\mathbf{C}\|_* \quad (4.3)$$
$$s.t. \mathbf{F} = \mathbf{C} + \mathbf{E}$$

where $\|\mathbf{C}\|_*$ is the nuclear norm, i.e. the sum of singular values of $\mathbf{C}$, and λ is a non-negative real number to control the trade-off between sparsity of $\mathbf{E}$ and nuclear norm of $\mathbf{C}$. For our purpose of realising model in (4.1), we find a suitable value for λ such that $rank(\mathbf{C}) = 4$. Another possible route is through coherent pursuit (CoP)[16], which finds the fixed rank subspace from a given number of lest coherent samples from the data. We found that CoP is inferior to RPCA for our purpose in terms of the performance statistics. Therefore we choose RPCA as our solver for our model in (4.1). We use $\mathbf{C}$, the outcome of (4.1), as the final output for performance evaluation in our experiments.

5. Experiment Evaluation

We ran through two echocardiography videos of two subjects resting in the supine position and apply ADASPAS, ADASPAS with fixed rank PCA, written as ADASPAS$^+$, and active contour based method [7] as a comparison study. Two echocardiography videos were collected during ultrasound scanning at 25 frames per second and, thus, the number of frames analysed was a function of this frame rate, heart rate, and number of cardiac cycles, i.e. sequences of systole, diastole, systole and so on. For these two videos, we have several cardiac cycles labelled by the expert physiologist as ground truth. The measurement of the size of the LV area is the quantity of interest, which we compare quantitatively.

Fig. 8 shows the estimated LV area measurements as pixel counts. Note that for data set 1 we have 4 full cardiac cycles although there are gaps between cycles. ADASPAS family follow the true LV area measurements much better than active contour method, and most importantly it reveals the cardiac cycles, i.e. the diastole and systole waves quite well. However, active contour method has much less variation and consistently underestimates LV area, showing cycles very weakly. Data set 2 contains one and half continuous cycles. Similar to data set 1, ADASPAS result is closer to true measurements while active contour method is a consistent overestimate. This set is very challenging as in most frames, a quarter of the LV wall and mitral valve pixels are missing. Thus it is very difficult for active contour method not to "leak out" to non-LV areas so that it included quite a lot of non-LV pixels. Fig. 9 shows the problem quite clearly. On data set 2, active contour failed to hold at the gap created by missing mitral valve while ADASPAS and ADASPAS$^+$ closed it up successfully in most cases.

We quantify the results by mean error, standard deviation of error (Std), correlation (Corr) and R^2 (R-squared) values between the estimated LV area measurements and the true values. The error is rescaled by true value. For mean and Std, the smaller the absolute value the better. For Corr, the larger

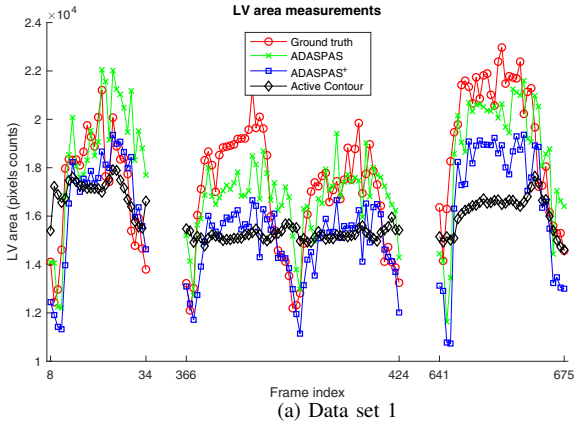

(a) Data set 1

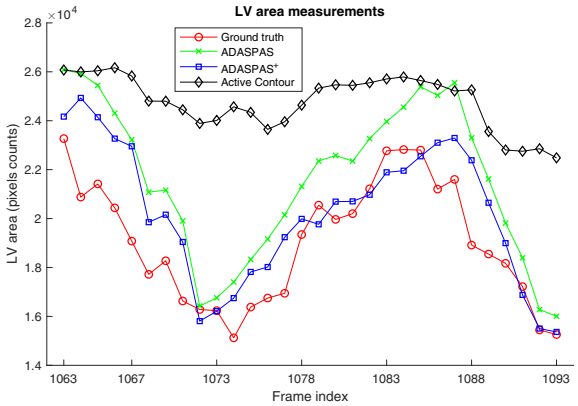

(b) Data set 2

Fig. 8: LV area tracking on two echocardiography videos. ADASPAS is consistently better than active contour method.

the better. For R^2, the closer to 0 the better. These statistics together describe how well the estimated values are predicting the true values.

TABLE I: Statistics of the performance of two methods

Data set	Method	Mean	Std	Corr	R-squared
Set 1	ADASPAS	0.011246	0.11829	0.70051	0.46858
	ADASPAS$^+$	-0.099629	0.091464	0.77694	0.10974
	AC	-0.083212	0.14287	0.35161	-0.34201
Set 2	ADASPAS	0.13116	0.062314	0.93117	-0.3178
	ADASPAS$^+$	0.063467	0.073359	0.86073	0.43797
	AC	0.3153	0.13204	0.79224	-4.9467

Table I summarises the results. ADASPAS family outperforms active contour method in all statistics. We need to point out that all methods ran through the whole video from frame 1 and only labelled frames were used for comparison. For ADASPAS family, a centre point was given and fixed for both videos while for active contour method, a starting LV, which is a manual labelled LV on frame 1 was given as initial contour and its estimated LV on one frame is used as initialisation for next frame. In this sense, active contour method used more information to start and also temporal information to track,

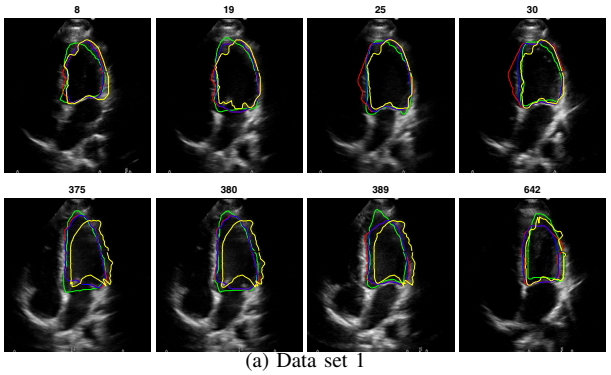

(a) Data set 1

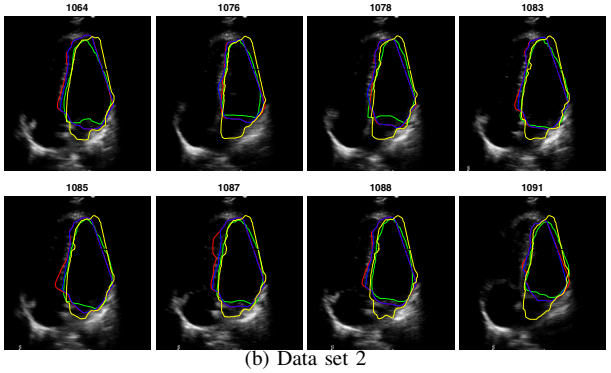

(b) Data set 2

Fig. 9: LV contours obtained by different methods on image frames from two echocardiography videos. Green curve is the ground truth, red is by ADASPAS, blue ADASPAS$^+$ and yellow active contour.

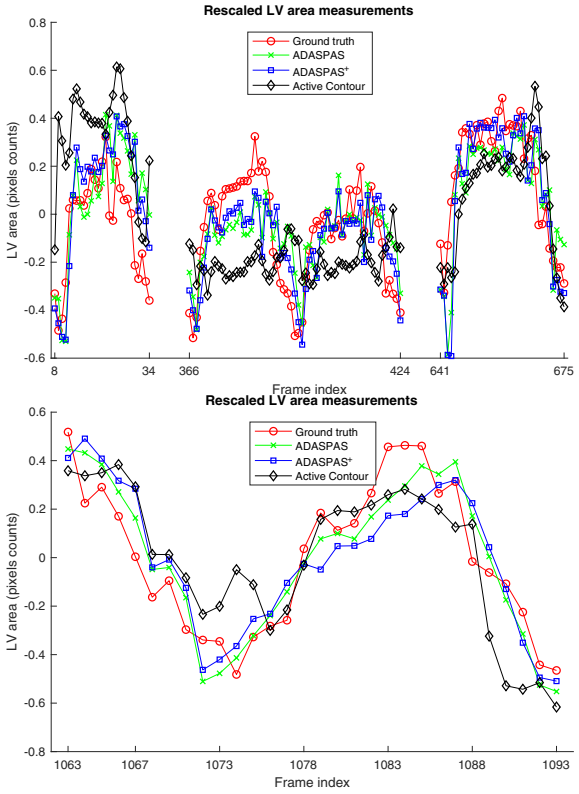

Fig. 10: LV area measurements after rescaling. ADASPAS family are still better than active contour method.

TABLE II: Statistics of the performance of two methods after rescaling

Data set	Method	Mean	Std	Corr	R-squared
Set 1	ADASPAS	8.5877e-07	1.098e-05	0.70051	0.46858
	ADASPAS$^+$	4.0401e-07	9.9076e-06	0.77694	0.10974
	AC	1.4925e-06	1.7956e-05	0.35161	-0.34201
Set 2	ADASPAS	4.5909e-08	6.0364e-06	0.93117	-0.3178
	ADASPAS$^+$	3.1979e-07	7.9466e-06	0.86073	0.43797
	AC	4.4367e-07	1.0917e-05	0.79224	-4.9467

way more information than what was available for ADASPAS family. Even so, it is far less accurate. Moreover, ADASPAS family are much faster than active contour. In our experiment, it cost only a tenth of what active contour needed to run through all frames in a video.

From Fig. 8 we see that active contour results contain cycles that might actually get the cardiac cycle right after rescaling. To verify this, for each measurement, we remove the mean and rescale by dividing the range. Note that the mean and range are taken from all measured LV area values by an algorithm in comparison. This operation is to match the measurement regardless the scales. Rescaling could be useful if the study of the echocardiography is to monitor heart performance under different conditions, for example with or without strenuous exercises. Fig. 10 shows the rescaled measurements with ground truth, where we see much better alignment. However, results from ADASPAS family are better in terms of matching cardiac cycles. Again, this visual observation is quantified by previously mentioned statistics in Table II. Although active contour results improve a lot after rescaling reflected by better statistics, it is still significantly inferior to those from ADASPAS family.

Fig. 9 shows only a handful of actual LV contours obtained by different methods. We run the previous statistics used to quantify measured LV areas on estimated LV contours and summarise in bar plot shown in Fig. 11. For each frame, we estimate LV contour using all algorithms and compute their performance statistics referring to ground truth. Then for each statistic, we calculate the mean and standard deviation to quantify the overall performance of a method. These summarising statistics are visualised as bar plot in Fig. 11, where the height of bar is the mean of that performance statistic across all frames, with error bars on top, which is the standard deviation of that performance statistic. Not that although Corr and R-squared are between 0 and 1, Mean and Std vary greatly. So for every performance statistic, we rescale the maximum to be 1 and apply the same scaling factor to standard deviation so that in Fig. 11 the highest bar in each performance statistic is always one, which better shows the performance differences. Note that for Mean and Std, the lower the better while for

Corr and R-squared, the larger the better.

It is very clear that ADASPAS$^+$ is leading in most of performance statistics, meaning that the fixe rank PCA does some positive adjustment to the contours estimated by ADASPAS, which is also evident in Fig. 9 where we can see that ADASPAS$^+$ corrected the contour of that from ADASPAS, for example on frame 25 and 30. So ADASPAS$^+$ LV contour estimation is closer to the truth than others.

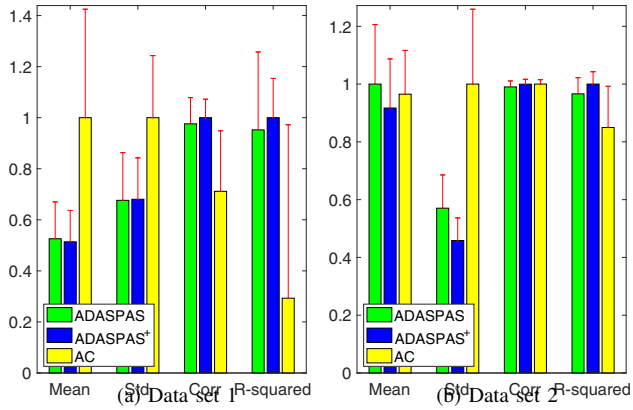

(a) Data set 1 (b) Data set 2

Fig. 11: Evaluation of LV contours obtained by different methods on image frames from two echocardiography videos. Green bars are for ADASPAS, blue for ADASPAS$^+$ and yellow active contour. The height of the solid bar the mean of the statistic, and the red bar on top is the standard deviation of the statistic. The maximum among each statistics is rescaled to 1 for visualisation purpose.

6. Conclusions

We proposed adaptive sparse smoothing (ADASPAS) with a fixed rank PCA for left ventricle volume measurement problem in this paper. It works on polar coordinates where the left ventricle contour identification is converted into a function smoothing problem. It requires very "light" image preprocessing and it is able to smooth out large spiky noise as well as large gaps caused by missing wall pixels. After the LV contour of each frame is extracted, a fixed rank PCA is applied to further smooth the estimated contours. Our experiment results showed that the proposed algorithms outperformed active contour method by large margin requiring much less information.

References

[1] Ismail Ben Ayed, Shuo Li, and Ian Ross. Embedding overlap priors in variational left ventricle tracking. *IEEE Transactions on Medical Imaging*, 28(12):1902–1913, 2009.

[2] Ismail Ben Ayed, Yingli Lu, Shuo Li, and Ian Ross. Left ventricle tracking using overlap priors. In *International Conference on Medical Image Computing and Computer-Assisted Intervention*, pages 1025–1033. Springer, 2008.

[3] Daniel Barbosa, Denis Friboulet, Jan D'hooge, and Olivier Bernard. Fast tracking of the left ventricle using global anatomical affine optical flow and local recursive block matching. *Proceedings of the MICCAI Challenge on Endocardial Three-dimensional Ultrasound Segmentation-CETUS*, pages 17–24, 2014.

[4] Emmanuel J. Candès, Xiaodong Li, Yi Ma, and John Wright. Robust principal component analysis? *Journal of the ACM*, 58(3):11:1–11:37, June 2011.

[5] Emmanuel J. Candès, Michael B. Wakin, and Stephen P. Boyd. Enhancing sparsity by reweighted ℓ_1 minimization. *Journal of Fourier Analysis and Applications*, 14(5):877–905, Dec 2008.

[6] G. Carneiro and J. C. Nascimento. Multiple dynamic models for tracking the left ventricle of the heart from ultrasound data using particle filters and deep learning architectures. In *2010 IEEE Computer Society Conference on Computer Vision and Pattern Recognition*, pages 2815–2822, June 2010.

[7] Tony F Chan and Luminita A Vese. Active contours without edges. *IEEE Transactions on image processing*, 10(2):266–277, 2001.

[8] Osama S Faragallah, Ghada Abdel-Aziz, and Hamdy M Kelash. Efficient cardiac segmentation using random walk with pre-computation and intensity prior model. *Applied Soft Computing*, 61:427–446, 2017.

[9] Junbin Gao, P. W. Kwan, and Y. Guo. Robust multivariate L1 principal component analysis and dimensionality reduction. *Neurocomputing*, 72:1242–1249, 2009.

[10] Bernard J. Gersh. *Mayo Clinic Heart Book*. William Morrow, 2000.

[11] Huang Lidong, Zhao Wei, Wang Jun, and Sun Zebin. Combination of contrast limited adaptive histogram equalisation and discrete wavelet transform for image enhancement. *IET Image Processing*, 9(10):908–915, 2015.

[12] Jun Liu, S. Ji, and Jieping Ye. SLEP: Sparse learning with efficient projection. Technical report, Arizona State University, 2009.

[13] Sotiris Malassiotis and Michael G. Strintzis. Tracking the left ventricle in echocardiographic images by learning heart dynamics. *IEEE Transactions on Medical Imaging*, 18(3):282–290, 1999.

[14] Nikos Paragios. A level set approach for shape-driven segmentation and tracking of the left ventricle. *IEEE transactions on medical imaging*, 22(6):773–776, 2003.

[15] Sandro Queiros, Joao Vilaca, Pedro Gonalves Morais, Jaime C. Fonseca, Jan D'hooge, and Daniel Barbosa. Fast left ventricle tracking in cmr images using localized anatomical affine optical flow. In *Progress in Biomedical Optics and Imaging - Proceedings of SPIE*, volume 9413, 02 2015.

[16] Mostafa Rahmani and George K Atia. Coherence pursuit: Fast, simple, and robust principal component analysis. *IEEE Transactions on Signal Processing*, 65(23):6260–6275, 2017.

[17] MG Strintzis, X Magnisalis, C Kotropoulos, I Pitas, and N Maglaveras. Maximum likelihood signal adaptive filtering of speckle in ultrasound b-mode images. In *Engineering in Medicine and Biology Society, 1992 14th Annual International Conference of the IEEE*, volume 5, pages 1870–1871. IEEE, 1992.

[18] Lin Yang, Bogdan Georgescu, Yefeng Zheng, Yang Wang, Peter Meer, and Dorin Comaniciu. Prediction based collaborative trackers (pct): A robust and accurate approach toward 3d medical object tracking. *IEEE Transactions on Medical Imaging*, 30(11):1921–1932, 2011.

[19] Xuli Zong, Andrew F Laine, and Edward A Geiser. Speckle reduction and contrast enhancement of echocardiograms via multiscale nonlinear processing. *IEEE transactions on medical imaging*, 17(4):532–540, 1998.